Integrated Cross-Species Translation and Biophysical Multi-Scale Modeling Links Molecular Signatures and Locomotory Phenotypes in Spaceflight-Induced Sarcopenia

Authors and Affiliations: Brendan K. Ball[1,2+*], Hammad F. Khan[2+*], Jee Hyun Park[2], Krishna Jayant[2], Deva D. Chan[2-3], Douglas K. Brubaker[4-5*]

1. Department of Pathology, Stanford University School of Medicine, Stanford, CA, USA
2. Weldon School of Biomedical Engineering, Purdue University, West Lafayette, IN, USA
3. School of Mechanical Engineering, Purdue University, West Lafayette, IN, USA
4. Center for Global Health & Diseases, Department of Pathology, Case Western Reserve University School of Medicine, Cleveland, OH, USA
5. Blood Heart Lung Immunology Research Center, University Hospitals, Cleveland, OH, USA

[+]These authors contributed equally to this work for co-first authorship

*Correspondence: khan332@purdue.edu, bbkazu@stanford.edu, dkb50@case.edu

Keywords: Spaceflight, sarcopenia, transcriptomics, locomotion, translational modeling, systems biology

ABSTRACT

Age-related skeletal muscle deterioration, referred to as sarcopenia, poses significant risks to astronaut health and mission success during spaceflight, yet its multisystem drivers remain poorly understood. While terrestrial sarcopenia manifests gradually through aging, spaceflight induces analogous musculoskeletal decline within weeks, providing an accelerated model to study conserved atrophy mechanisms. Here, we introduced an integrative framework combining cross-species genetic analysis with physiological modeling to understand mechanistic pathways in space-induced sarcopenia. By analyzing rodent and human datasets, we identified conserved molecular pathways underlying microgravity-induced muscle atrophy, revealing shared regulators of neuromuscular signaling including pathways related to neurotransmitter release and regulation, mitochondrial function, and synaptic integration. Building upon these molecular insights, we developed a physiologically grounded central pattern generator model that reproduced spaceflight-induced locomotion deficits in mice. This multi-scale approach established mechanistic connections between transcriptional changes and impaired movement kinetics while identifying potential therapeutic targets applicable to both spaceflight and terrestrial aging-related muscle loss.

INTRODUCTION

Space exploration is rapidly developing with the increasing number of missions to the International Space Station and beyond. As humans push towards longer spaceflights and journeys to other planets, understanding the physiological changes due to space travel has become critical. Despite decades of active research, our understanding of the biological burden of spaceflight remains limited. Moreover, this limitation is further exacerbated by the effects of prolonged exposure to the microgravity environment[1] and cosmic radiation,[2,3] which has been proven to be detrimental to human health.[4]

A well-documented consequence of space exploration is the deterioration of musculoskeletal health. Astronauts who return from space experience muscle atrophy, impaired muscle performance, and loss of strength.[5,6] This process of muscle degradation resembles sarcopenia, a progressive age-related condition that often emerges over several decades and leads to muscle loss and function.[7] While this condition progresses over an individual's lifetime on Earth, the development of sarcopenia-like pathology is accelerated under microgravity conditions.[8] Despite noted observations of muscle and strength breakdown,[9] the exact mechanisms and pathways by which space-induced sarcopenia progresses are poorly understood.

There are major challenges to understanding how conditions in space affect human health. First, there are limited experimental samples and astronauts that have been studied on the International Space Station, often due to space constraints, costs, and accessibility.[10] This is important because studying physiological changes in space-like

conditions on Earth does not effectively translate to the harsh conditions in spaceflight. Additionally, astronauts on average spend 6 months per space mission tour, and thus there is limited information on the longer-term effects of space travel and sample size to study such effects.[11] To address this challenge, previous studies aimed to improve our understanding of spaceflight and sarcopenia through the use of *in vitro*[12] and *in vivo* rodent models.[13] Despite these efforts, these approaches did not account for the heterogeneity of the human population and the biological differences across mammalian species. As a result, our understanding of a mechanistic pathway to sarcopenia conditions is largely unknown.

To overcome this limitation, we leveraged a framework known as Translatable Components Regression (TransComp-R), a computational model that synthesizes multi-omics data from preclinical rodent models and human data to predict disease outcomes in humans.[14,15] The TransComp-R pipeline has been successfully applied to overcome other biomedical challenges including Alzheimer's disease,[16–20] osteoarthritis,[1] and inflammatory bowel disease.[14,21] We coupled this approach with a biophysically grounded model of central pattern generator (CPG) networks,[22,23] therefore enabling multiscale interrogation of sarcopenia.

In this study, we used TransComp-R to show that transcriptomics data from mouse models under spaceflight conditions predicts human sarcopenia outcomes. We performed cross-species computational modeling to synthesize spaceflight mouse and sarcopenia human data to identify potential biological pathways that are involved in

92 muscle degeneration. To link the observed space-related sarcopenia to neuromuscular
93 function, we built a network of leaky integrate-and-fire neurons to build a computational
94 CPG model that recapitulated locomotion kinetics in healthy conditions. Importantly,
95 incorporation of the predictive transcriptomic data into the model generated similar
96 phenotypic gait responses observed under sarcopenia conditions. Thus, this approach
97 enables an improved understanding of mechanisms associated with space-induced
98 sarcopenia and may inform therapeutic avenues for sarcopenia and other muscle-
99 deteriorating conditions related to spaceflight and on Earth.
100

101 **RESULTS**

102 **Mouse spaceflight principal components separate human sarcopenia and control**
103 **conditions**

104 We accessed RNA-sequencing spaceflight mouse data from the NASA Open Science
105 Data Repository (OSDR). The publicly available spaceflight dataset (OSD-103) contained
106 16-week-old C57BL/6J male mice with a sample size of n=6 ground controls and n=6
107 spaceflight conditions.[24,25] The spaceflight group was housed at the International Space
108 Station for 37 days before euthanasia and collection of quadricep muscle samples. The
109 ground control group was housed on Earth for reference. We then acquired RNA-
110 sequencing data of patients with sarcopenia from Gene Expression Omnibus (GEO). We
111 selected three separate cohort studies that studied sarcopenia among different racial
112 demographics, including Caucasian (GSE111006), Afro-Caribbean (GSE111010), and
113 Chinese (GSE111016) descent.[26,27] Our integration of multiple cohorts allowed us to
114 reference our findings across different human backgrounds.

We applied the TransComp-R model to identify principal components (PCs) that encoded transcriptomics variation of spaceflight mice that predicted sarcopenia outcomes in humans. The TransComp-R pipeline works by computing a mouse principal component analysis (PCA) space and projecting human data into space. Mouse PCs that encode transcriptomics capable of stratifying human disease from control groups are then identified by a regression model and can be biologically interpreted through pathway enrichment analyses and follow-up studies.

With the TransComp-R model, we first matched homologous gene pairs across the mouse and all three human datasets (**Figure 1a**). We next applied principal component analysis (PCA) on the mouse dataset to identify PCs that explained 80% of the cumulative variation and projected the human dataset with the Chinese cohort with sarcopenia and control conditions into the mouse PC space.

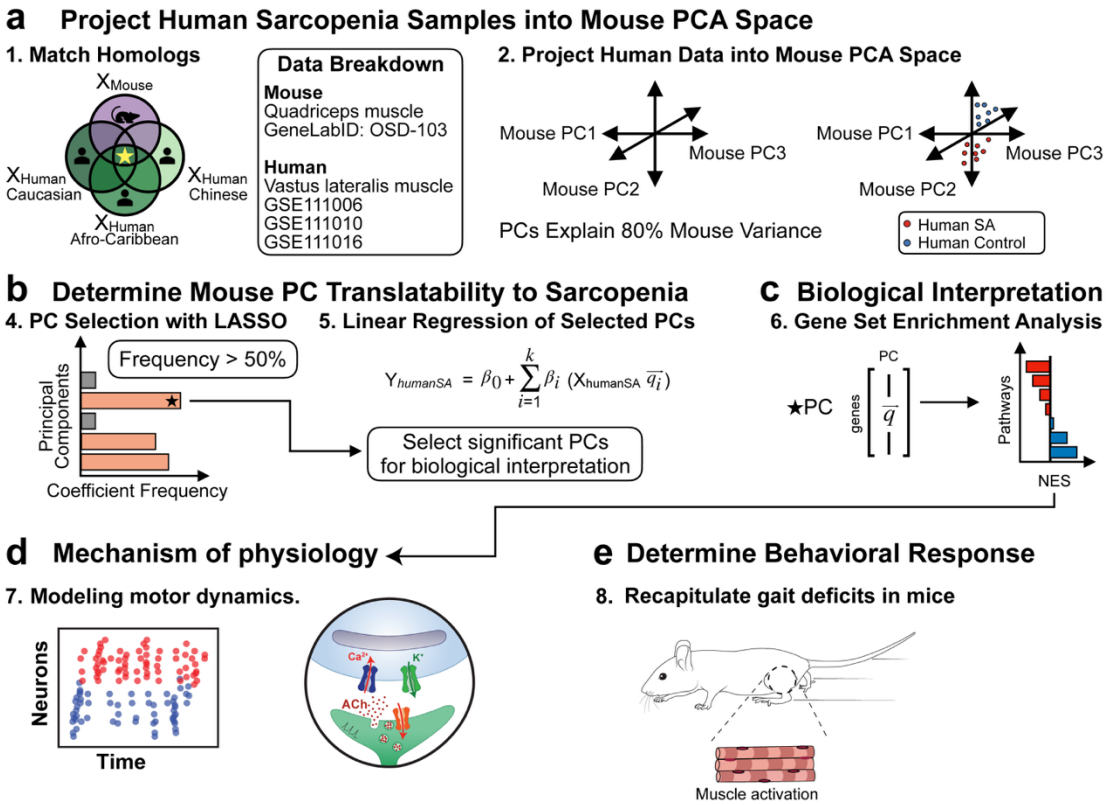

Figure 1. Mouse to human modeling workflow. (a) Homologous pairs between mouse and human are first matched. Human sarcopenia and control groups (Chinese cohort) are projected into the space flight mouse PCs. The human Caucasian and Afro-Caribbean cohorts were used for downstream validation analysis. **(b)** The PCs selected by LASSO are regressed against human sarcopenia and control outcomes to determine significance. **(c)** Significant PCs from the generalized linear model are used for downstream biological analysis. (**d**) Biophysical modeling of motor dynamics. (**e**) Recapitulate behavior deficits in space-induced sarcopenia based on genetic determinants.

After synthesizing the mouse and human transcriptomics data together, we selected PCs that were relevant in predicting human sarcopenia condition with LASSO (least absolute shrinkage and selection operator) (**Figure 1b**). The selected PCs from LASSO were used in a generalized linear regression against human sarcopenia and control groups. The significant PCs were then interpreted using gene set enrichment analysis (GSEA). Lastly, we validated our findings with the Caucasian and Afro-Caribbean cohorts that also contained sarcopenia and control data.

After matching for homologous pairs, we identified 12,484 genes shared across the mouse and human datasets. We constructed a mouse PCA space and projected the Chinese cohort and identified 7 PCs that explained 80% of the variance (83.4% var. exp). We next calculated how much variance the mouse PCs explained in the human data to understand the potential of translation from mouse to human (**Figure 2a**). Among the seven mouse PCs, we found PC1, PC3, and PC6 explained a higher ratio of human variance compared to mouse variance. This finding suggests that PC1, PC3, and PC6 may have a more pronounced ability to capture variance across species than other PCs.

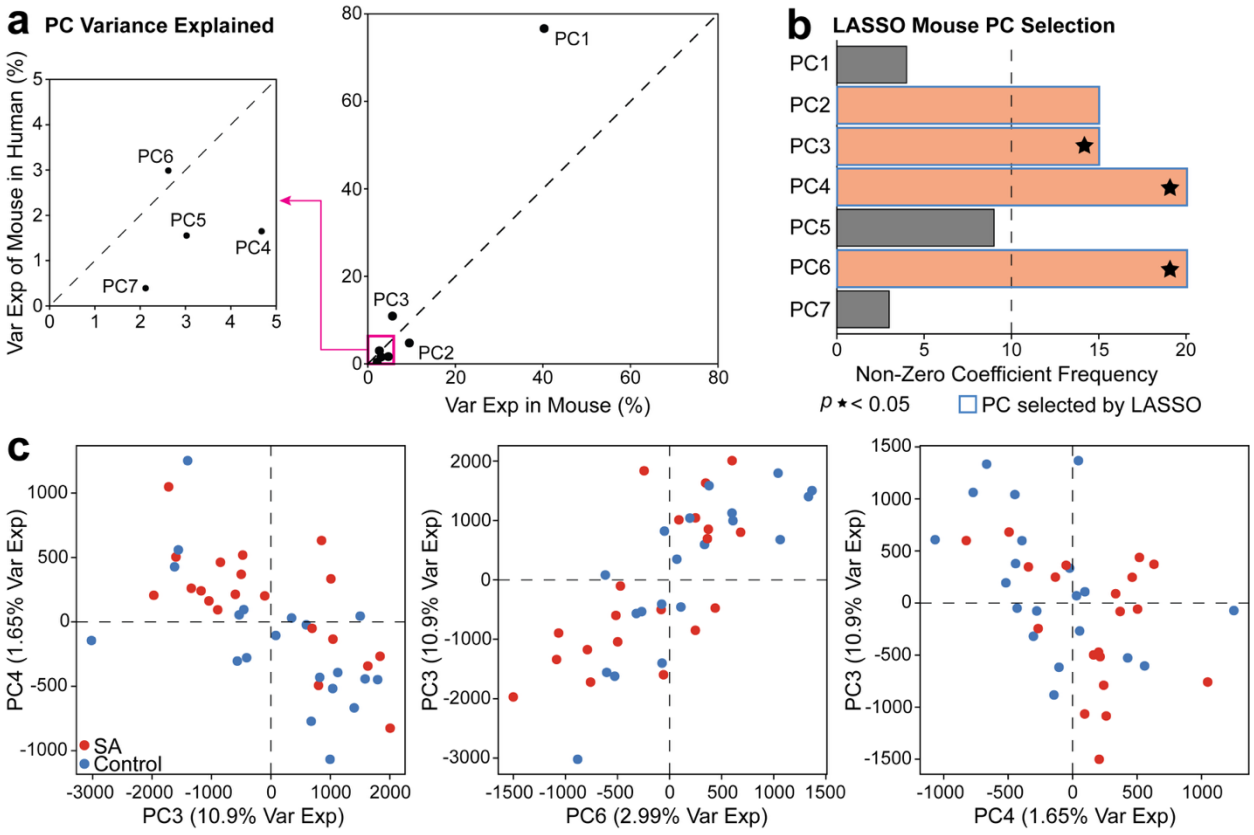

Figure 2. Significant mouse PCs distinguish sarcopenia and control conditions in humans. (a) The percent variance explained of mouse PCs and how much they explain in human data. **(b)** PC selection using the LASSO. PCs selected by LASSO that were significant in a GLM (p value < 0.05) are denoted with a star. **(c)** Plots of significant mouse PCs separating sarcopenia and control in humans (SA=sarcopenia).

Of the seven PCs, we identified PC2, PC3, PC4, and PC7 with our LASSO model (selected more than half of the twenty random rounds) to be relevant eigenvectors with power to stratify human sarcopenia and control patients (**Figure 2b**). We created a generalized linear regression model incorporating these four PCs and found PC3, PC4, and PC6 to be significantly separating the sarcopenia and control groups ($p = 0.0286$, 0.0371, and 0.0253, respectively). We next visualized the three significant PCs and found that the transcriptomics variation encoded on each PC separated the human sarcopenia and control groups (**Figure 2c**).

Metabolic and immune-associated pathways on cross-species principal components distinguish patients with sarcopenia

Having identified significant murine PCs that distinguish between human sarcopenia conditions, we conducted GSEA on the PC loadings and identified pathways related to neuroactive ligand receptor interactions, immune pathways, and cellular structures enriched for human sarcopenia on mouse spaceflight PC3 (**Figure 3a**). Genes that were involved with neurodegenerative diseases and metabolic pathways were associated with healthy human groups. This indicates that these genes may become disrupted under sarcopenia conditions and encode human phenotype predictive cross-species biological signatures.

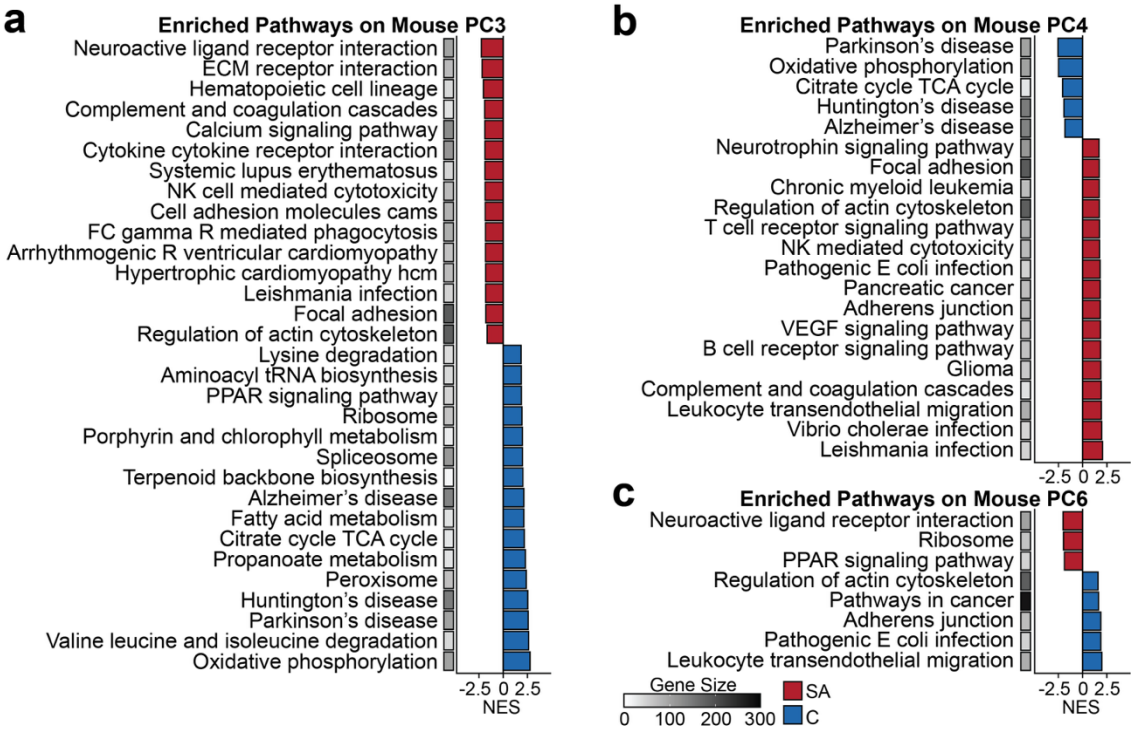

Figure 3. KEGG pathway enrichment analysis. Biological pathways enriched on **(a)** PC3, **(b)** PC4, and **(c)** PC6. All pathways are significant with a Benjamini-Hochberg adjusted p<0.01. The gene size represents the number of genes enriched in the biological pathway. Pathways are shown with associations to human sarcopenia (red) and control (blue) based on the directionality of separation for each PC. The bar plots are represented by their respective normalized enrichment score (NES). (SA=sarcopenia, C=control).

On the mouse spaceflight PC4, we found pathways involved with immune signaling and cellular structure to be enriched in the sarcopenia group (**Figure 3b**). Among the pathways enriched on PC6, we found neuroactive ligand receptor interaction and PPAR signaling associated with sarcopenia, whereas regulation of actin cytoskeleton, adherens junction, and leukocyte transendothelial migration were enriched in control (**Figure 3c**).

We also performed GSEA using the hallmark curation and found signaling mechanisms involved with the immune system to be involved with sarcopenia (**Supplementary Figure 1**). Additionally, we found oxidative phosphorylation to be consistently enriched for the

198 control group in PC3, PC4, and PC6. Such results further support our findings with the
199 reported KEGG pathway analysis. These findings also show that genes contributing to
200 the immune responses, as well as mitochondrial function associated with oxidative
201 phosphorylation may play important roles in the muscle degenerative process associated
202 with sarcopenia in humans and can be measured in a predictive capacity in murine
203 spaceflight models.
204
205 **Significant PC gene loadings from the Chinese cohort are translatable to**
206 **Caucasian and Afro-Caribbean demographics**
207 After identifying biological pathways associated with sarcopenia and control, we assessed
208 whether our findings generalized across human demographic groups. We constructed
209 three PLS-DA models using combined Caucasian and Afro-Caribbean human sarcopenia
210 data and genes extracted from each significant mouse spaceflight PC (PC3, PC4, PC6)
211 that our TransComp-R model as having cross-species predictive value in the Chinese
212 cohort. Our objective was to see whether the biological signatures identified in the
213 significant cross-species PC's of TransComp-R could generalize to other demographic
214 groups.
215
216 We combined the Caucasian and Afro-Caribbean sarcopenia datasets to determine if
217 findings from these populations were also reflected by our findings from the Chinese
218 cohort. The Caucasian and Afro-Caribbean datasets contained further annotations on
219 muscle weakness in the subjects beyond those reported in the Chinese cohort. We first
220 excluded control patients with any reported history of muscle weakness or muscle loss to

221 avoid confounders. We combined the Caucasian and Afro-Caribbean datasets model and
222 verified that batch effects were not present with PCA (**Supplementary Figure 2**).
223 Breaking down the combined and processed demographics, we analyzed n=28 healthy
224 Caucasians (Age: 72.6±2.3 standard deviations), n=4 sarcopenia Caucasians (Age:
225 74.3±3.6), n=14 Afro-Caribbean (76.4±7.4), and n=9 sarcopenia Afro-Caribbean
226 (76.8±7.9) individuals.
227
228 We selected a panel of genes for each model from each TransComp-R identified PC,
229 selecting the top 10 and bottom 10 genes ranked by their murine PC loadings, for PLS-
230 DA predicting human sarcopenia vs. control groups in the combined Caucasian and Afro-
231 Caribbean dataset. Genes strongly contributing to the model contained a calculated
232 variable importance of projection (VIP) score greater than 1.
233
234 We demonstrated a separation of control and sarcopenia with the combined human
235 dataset (**Figure 4a**). With murine spaceflight PC3 genes, the human samples were
236 separated among the first latent variable (LV). On this LV, we found genes that are
237 strongly associated with sarcopenia, which included *DLG3*, *CALB2*, *LHFPL6*, and
238 *ADAM33* (**Figure 4b**). The *DLG3* and *CALB2* genes are associated with neuron signaling,
239 whereas *LHFPL6* and *ADAM33* are involved with cell-to-cell signaling and
240 communication. Oppositely, genes such as *PPP1R12B* and *CNTF are associated* with
241 the control groups. These genes are involved in helping muscle contraction through
242 myosin phosphatase activity and enhancing survival factors for neuronal cells,
243 respectively.

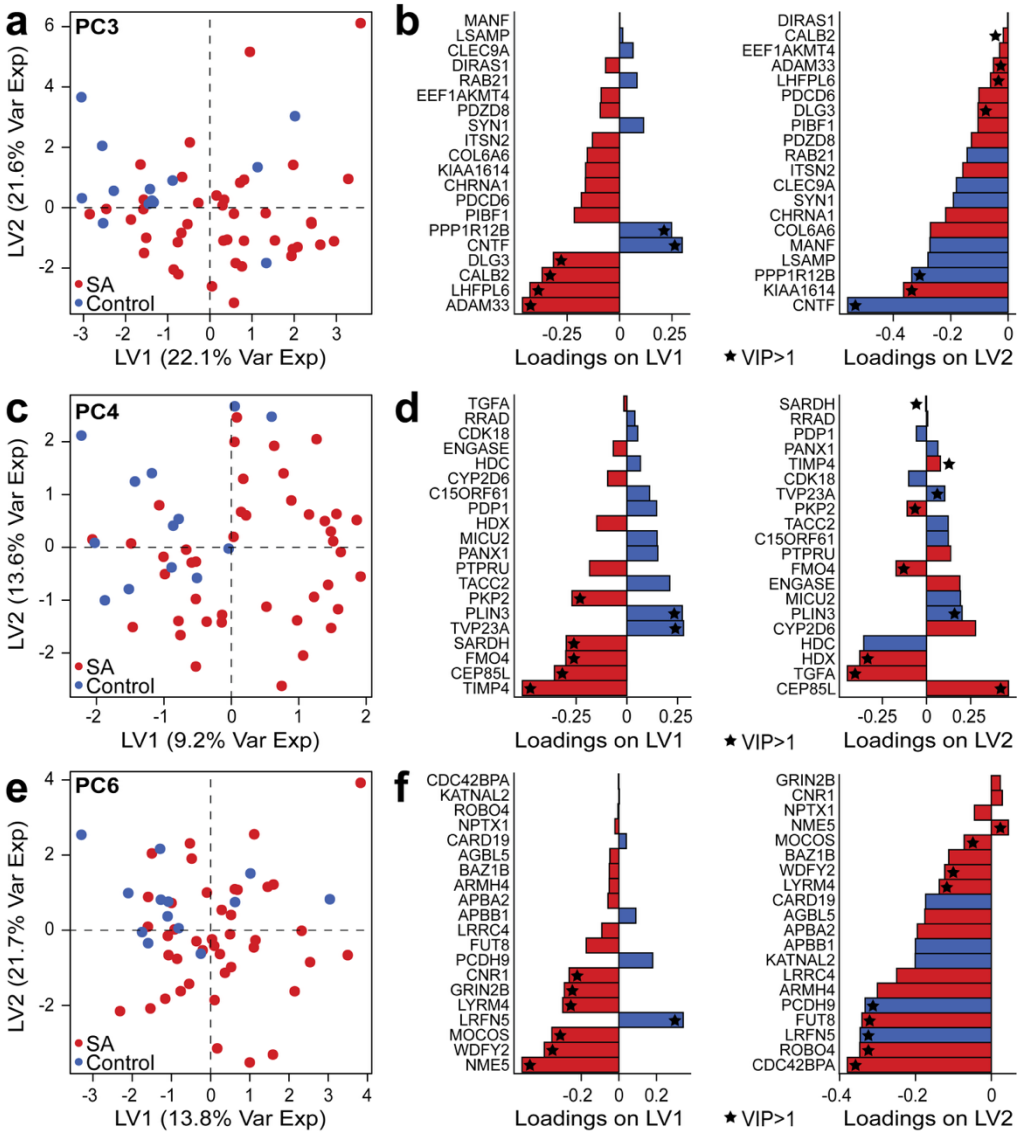

Figure 4. Gene expression driving separation among Chinese sarcopenia cohorts is also reflected in Caucasian and Afro-Caribbean populations. (a) PLS-DA on the top 10 and bottom 10 genes identified in the spaceflight PC3. **(b)** The loadings of the first two latent variables for PC3. **(c)** PLS-DA for PC4. **(d)** Loadings for PC3. **(e)** PLS-DA for PC6. **(f)** Loadings for PC6. Loadings with a VIP>1 are labeled with a star. The color on the loadings represents the highest contribution to sarcopenia or control by the specific gene. (SA=sarcopenia).

We also performed PLS-DA on mouse spaceflight PC4 genes and demonstrated that LV1 discriminated between the control and sarcopenia human groups (**Figure 4c**). We identified *PKP2*, *SARDH*, *FMO4*, *CEP85L*, and *TIMP4* genes to associate with

256 sarcopenia, whereas *PLIN3* and *TVP23A* were associated with control (**Figure 4d**).
257 These genes have known associations with cellular structure, metabolism, and vesicle
258 transport. For murine spaceflight PC6, we similarly found the control group clustered on
259 the negative score of LV1, and the sarcopenia group clustered among positive scores
260 (**Figure 4e**). This separation was defined by *CNR1*, *GRIN2B*, *LYRM4*, *MOCOS*, *WDFY2*,
261 and *NME5* for sarcopenia. For the control groups, we found *LRFN5* as the only gene
262 contributing to the PLS-DA separation with a VIP>1. Interestingly, the *CNR1* and *GRIN2B*
263 genes are linked to neurotransmission and brain function whereas *LYRM4* and *MOCOS*
264 are connected to mitochondrial metabolism.[28–30] The *LRFN5* gene we found associated
265 with the control group is associated with cell-to-cell communication among neuronal cells.
266

267 **In silico drug screening analysis identifies candidate potential therapeutics for**
268 **preventing spaceflight-associated sarcopenia**

269 After confirming these mouse PCs are reflective in sarcopenia across multiple human
270 demographics, we leveraged a computational correlation analysis to shed light on
271 potential therapeutics associated with space-induced sarcopenia. We used the Library of
272 Integrated Network-Based Cellular Signatures (LINCS) Consensus Signatures that
273 contains characteristic direction coefficients based on gene expression profiles of 33,609
274 drugs.[31] We analyzed 2,558 of these drugs after excluding duplicates and those that did
275 not contain any reported cellular targets. We used a Spearman's correlation analysis
276 between the characteristic direction coefficient values of affected genes from a respective
277 drug to the loadings on selected mouse PCs. Our goal was to determine medications that
278 may have potential therapeutic benefits by identifying drugs that induced gene signature

279 changes opposite to the transcriptomics profile of spaceflight-induced sarcopenia. Here,
280 we focused on significant drugs that were approved by the Food and Drug Administration
281 (FDA) to ensure our findings were met with standards for safety and effectiveness.
282
283 We found 135 drugs significantly correlated with the gene loadings encoded on the mouse
284 PC3 (**Figure 5a**). We consulted the 135 drugs to the FDA Orange Book (March 2025
285 version) and determined 37 FDA-approved drugs. From the selected FDA-approved
286 drugs, isradipine had the highest correlation coefficient of 0.2246 and is used to treat
287 hypertension through calcium channel blockers. We also found mestinon (ρ=0.2184), a
288 medication primarily used for muscle weakness condition in myasthenia gravis, and
289 sunitinib (ρ=0.2003), an anti-cancer medication, as drugs associated with reversing the
290 sarcopenia gene signatures. Among the drugs with the highest association of inducing
291 sarcopenia-like gene expressions, we found two medications used to treat schizophrenia
292 (ariprazole, ρ=-0.1958, and lurasidone, ρ=-0.1689), and temsirolimus (ρ=-0.1756), used
293 for renal cell carcinoma.

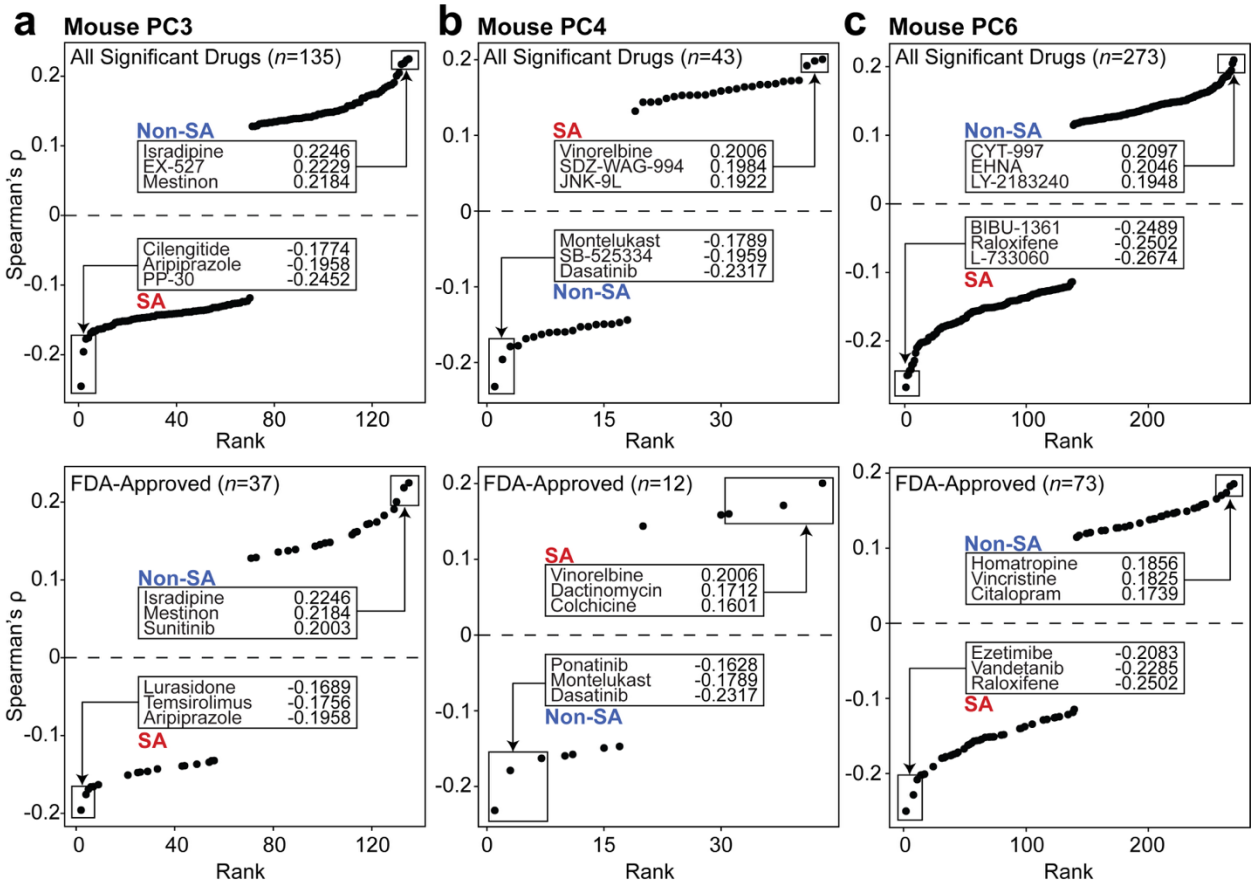

Figure 5. Gene expression correlational analysis for therapeutic discovery. All significant drugs and a subset of significant drugs selected by their FDA-approval status for **(a)** mouse PC3, **(b)** mouse PC4, and **(c)** mouse PC6. The top and bottom three medications ranked by their Spearman's ρ value are labeled by sarcopenia (signatures correlated to genes elevated in sarcopenia) or non-sarcopenia (signatures correlated to genes elevated in healthy conditions). (SA=sarcopenia, Non-SA=healthy condition).

On mouse PC4, we identified 43 significant drugs associated with spaceflight induced sarcopenia gene expression, 12 of which were FDA-approved (**Figure 5b**). Dasatinib, a chemotherapy drug used to treat cases of leukemia, had the most negative correlation score (ρ=-0.2317). Other medications that correlated with the non-sarcopenia profile included montelukast (ρ=-0.1789, treats asthma symptoms) and ponatinib (ρ=-0.1628, chronic myeloid leukemia treatment). The FDA-approved medications that most associated with sarcopenia-like conditions included vinorelbine (chemotherapy for non-

309 small cell lung cancer), dactinomycin (chemotherapy medication), and colchicine (anti-
310 inflammatory to treat gout attacks).
311
312 With mouse PC6, we identified 273 significant drugs, 73 of which were FDA-approved.
313 Homatropine (ρ=0.1856), vincristine (ρ=0.1825), and citalopram (ρ=0.1739) were among
314 the drugs with the highest correlation to reversing spaceflight-induced sarcopenia gene
315 expression profiles. These medications are used for muscarinic acetylcholine receptor
316 antagonists, leukemia and cancers, and selective serotonin reuptake inhibitor
317 antidepressants, respectively. Conversely, medications with the highest associations to
318 inducing a spaceflight-induced sarcopenia disease signatures included raloxifene (ρ=-
319 0.2502), vandetanib (ρ=-0.2285), and ezetimibe (ρ=-0.2083). Raloxifene is used for
320 individuals undergoing menopause to address osteoporosis and breast cancer risk
321 reduction. Vandetanib and ezetimibe are used to treat medullary thyroid cancer and to
322 reduce high cholesterol levels in the blood, respectively.
323
324 **Multivariate analysis reveals rodent gait deficits related to orbital spaceflight**
325 Space-induced muscle atrophy represents a compelling model for investigating
326 fundamental mechanisms of sarcopenia, just as sarcopenia is a compelling disease
327 model for studying ways to prevent space-induced muscle atrophy. We demonstrated
328 with pathway enrichment analysis that neuroactive ligand receptor interaction and PPAR
329 signaling were associated with sarcopenia in both human and rodent models, suggesting
330 conserved genetic determinants for sarcopenia.[32] To further interrogate the relationship
331 between sarcopenia changes at the molecular level, we performed multivariate analysis

332 of locomotory deficits in rodents following prolonged microgravity exposure aboard the
333 International Space Station.
334
335 We accessed the spaceflight behavioral assay available on the NASA database (OSD-
336 478), which contains a prospective collection of gait data between mice undergoing
337 spaceflight in orbit aboard the ISS and ground control over 35 days.[33] Pre-flight and post-
338 flight gait measurements were conducted across a total of n=40 mice (n=20 mice per
339 group), measuring multiple aspects of locomotion and gait kinematics. We conducted an
340 unsupervised analysis of effects on gait dynamics across spaceflight and ground control
341 by projecting the data into a mouse PC subspace to extract behavior dynamics that were
342 most affected during spaceflight.
343
344 We used PCA of gait dynamics to reveal distinct behavioral signatures between pre- and
345 post-flight conditions (**Figure 6a, b**). We clustered the treatment groups based on chi-
346 squared confidence ellipse and noted a distinct separation in PC space that was more
347 pronounced in spaceflight groups compared to ground controls, suggesting specific
348 microgravity-induced adaptations across mice as opposed to temporal artifacts. The first
349 PC captured 25.5% of total variance followed by 14.8%, and 11.3%, for PC 2 and 3,
350 respectively. Approximately 80% of locomotory variation was explained by just eight
351 components (**Figure 6c**), suggesting strongly shared effects across all mice undergoing
352 spaceflight.
353

To investigate behavioral contributions, we conducted a loading analysis of tracked gait properties during locomotion and identified key gait parameters contribution to PC variance in the publicly available mouse data (**Figure 6d**). For example, among the first two components, we identified propulsion parameters and stride as primary contributors to observed variance (**Figure 6d**). We found similar results when conducting systematic testing across all gait parameters across mice (**Supplementary Figure 3**). To further quantify this, we selected the most contributing gait parameters across the first 4 PC components and performed inferential statistics across mice. We found significant alterations in propel time ($p=0.04$), stance time ($p=0.007$), stride length ($p<0.001$), and swing time ($p<0.001$) following orbital habitation (**Figure 6e**). These deficits suggest impairments in both stride generation and balance feedback mechanisms essential for coordinated movement.[34] Similar observations were noted in humans undergoing functional gait tests.[35] Moreover, this analysis demonstrated clear locomotor deficits in mice following spaceflight exposure. Notably, the propelling force and stride kinematics were strongly altered compared to ground control. These coordinated changes could suggest disruption in multiple neural pathways governing both balance maintenance and gait kinetics, consistent with functional adaptations to microgravity conditions.[35,36]

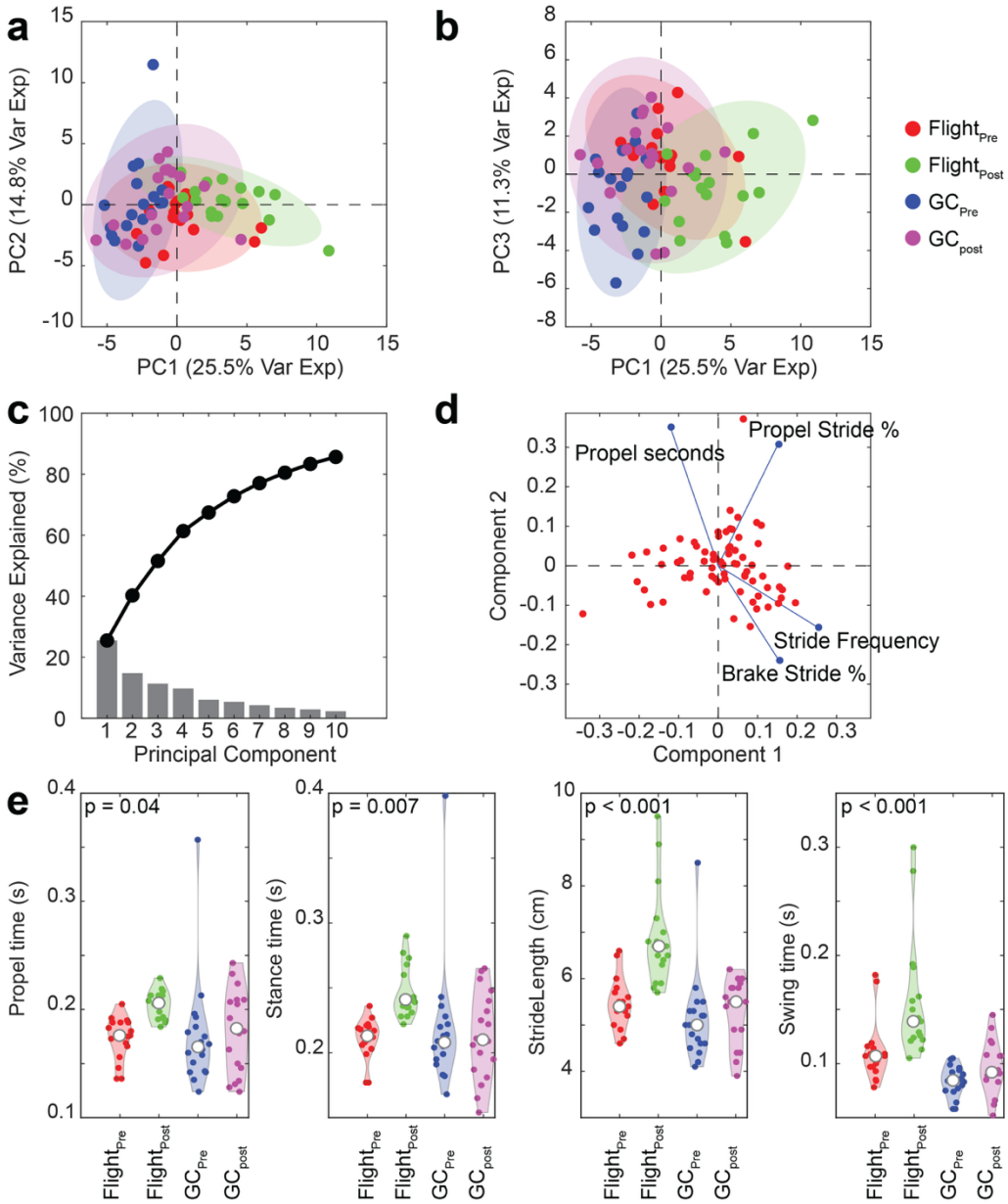

Figure 6. Behavioral alterations during spaceflight. (a) PC projection of the first and second component axis with behavioral variables under pre- and post-flight conditions with ground controls. **(b)** PC projection of the first and third PC components. **(c)** Scree plot of variance explained for the first 10 PC components. **(d)** A bi-polar plot of the top 4 variable behaviors among the flight and ground control groups. **(e)** Highest weighted behavioral alteration properties determined by PC analysis (n = 40 mice total, one-way ANOVA test).

382 **Physiological modeling of gait characteristics**

383 To understand the physiological mechanisms underlying space-induced locomotory
384 deficits and key molecular determinants of sarcopenia, we established a biologically
385 plausible physiological model that captured the essential dynamics of spinal locomotor
386 circuits under normal terrestrial conditions. This computational framework serves as a
387 substrate to later assess microgravity-induced alterations, demonstrating how changes in
388 biomolecular network activity directly translate to muscle function and ultimately to
389 observable gait parameters.

390

391 Our network model consisted of leaky integrate-and-fire neurons following well-
392 established membrane potential and gating dynamics.[22,23,37–39] To capture oscillatory
393 dynamics often found during locomotion, we assigned distinct flexor and extensor neural
394 populations that were inhibitory connected to one another. This enabled a subset of
395 neurons to generate patterned activity in the absence of input to both regions, thus
396 reflecting CPG dynamics (**Figure 7a**).[37] Simulation of the population model drove
397 characteristic oscillatory patterns in membrane potential dynamics between flexor and
398 extensor circuits under normal gravity conditions (**Figure 7b**), with flexors exhibiting more
399 rapid depolarization, consistent with their role in initiating limb movement. The
400 computational network successfully reproduced rhythmic activity reflecting central pattern
401 generators, with flexor neurons (red) showing synchronized burst patterns distinct from
402 extensor neurons (blue) during simulated normal locomotion (**Figure 7c**). We used the
403 cumulative output of each group to infer muscle activation patterns that were used to
404 extract gait dynamics (**Figure 7d**). Gait kinematics exhibited a strong phase-coherent

response (67%) between extensor and flexor periods (**Figure 7e**) reflecting coordination between muscle groups.

Thus, this computational approach creates a powerful platform connecting three levels of analysis: neuronal firing patterns, muscle activation dynamics, and resultant gait kinetics (**Figure 7f-h**). The normal phase relationships, stride distributions, and swing patterns established here provide quantifiable baselines against which space-induced neural adaptations can be measured in subsequent experiments. By bridging cellular neurophysiology to whole-organism locomotion, this model enables mechanistic investigations into how microgravity disrupts motor control at multiple biological levels.

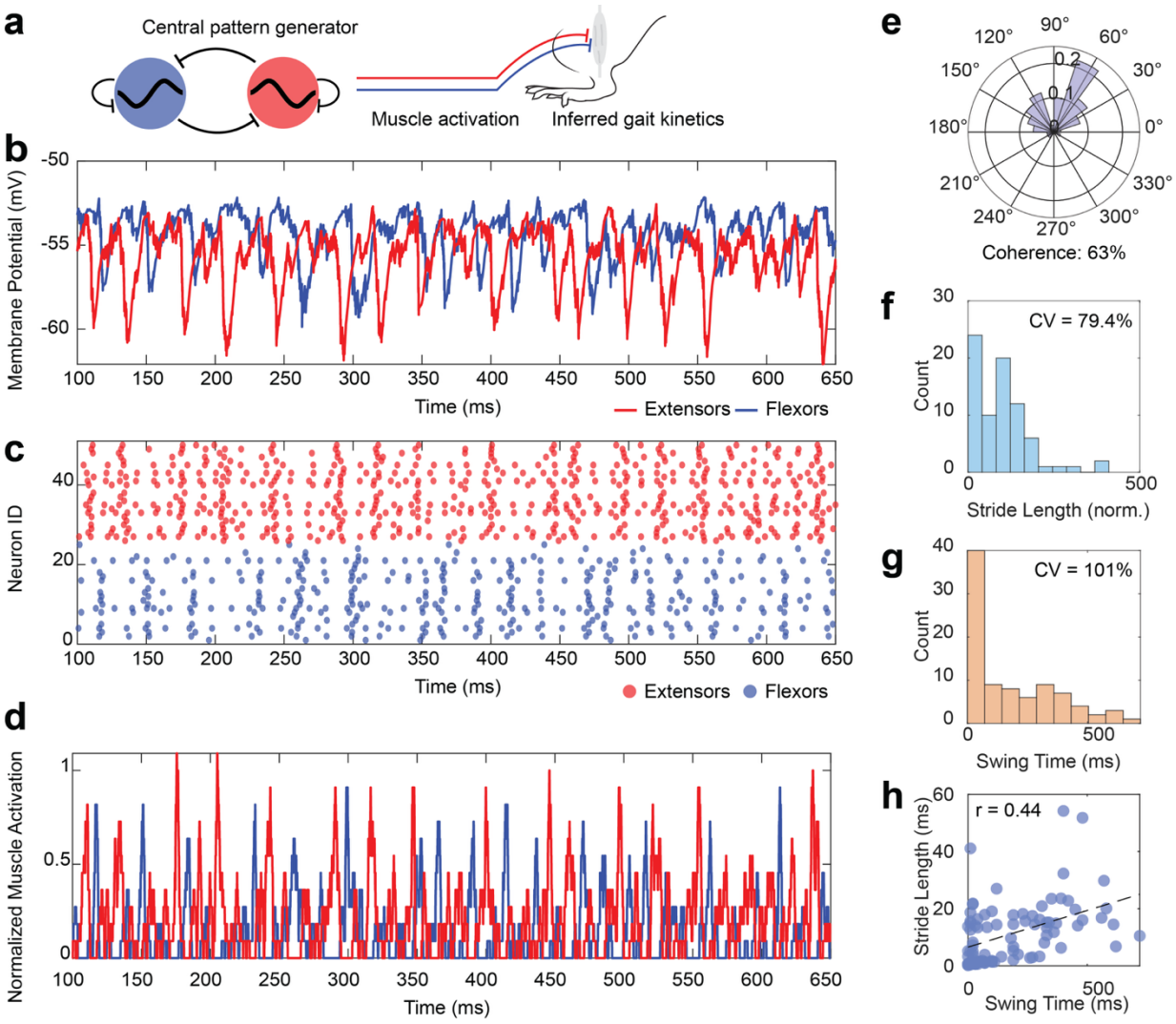

Figure 7. Motor neuron population model for locomotory behavior. (a) Schematic of the mechanistic physiological model. **(b)** Averaged population membrane dynamics from a leaky integrate-and-fire model. **(c)** Rastergram of 50 neurons spiking during constant input. Neurons are colored based on assigned flexor or extensor dynamics. **(d)** Inferred muscle activity patterns as a function of population output. **(e)** Polar plot of phase relationship between flexor and extensor population dynamics. **(f)** Distribution of stride length with coefficient of variation. **(g)** Distribution of swing times with coefficient of variation. **(h)** Regression of correlation swing time and stride length.

427 **Computational framework linking biomolecular determinants of sarcopenia to**
428 **altered gait characteristics**

429 To bridge the gap between the identified biomolecular determinants found by
430 TransComp-R's gene enrichment analysis and the physiology of gait characteristics, we
431 modified our network model to exhibit sarcopenia phenotypic behavior. This was primarily
432 informed by the identified ligand-gated genetic disruption (*GRIN2B* and *CNR1*), during
433 spaceflight in both mice and human cohorts (**Figure 8a**). We modified the synaptic
434 transmission probability and conductance, while biasing the total input variability, into the
435 network of individual neurons in both flexor and extensor populations **(Figure 8b**)**.** We
436 noted that, upon this disruption, an observed reduction in phase-coherence between
437 flexor and extensor dynamics compared to the healthy terrestrial network.
438 ($Coherence_{healthy}$ = 55%, $Coherence_{sarcopenia}$ = 33%, **Figure 8c**). The change in network
439 activity also drove a significant increase in both inferred gait swing time and stride length
440 ($p<0.0001$, **Figure 8d, e**), most likely due to increased variability in the CPG network.
441 Thus, these results recapitulate the same gait alterations observed in cohorts of mice that
442 spend a significant time in space flight (**Figure 6e**).

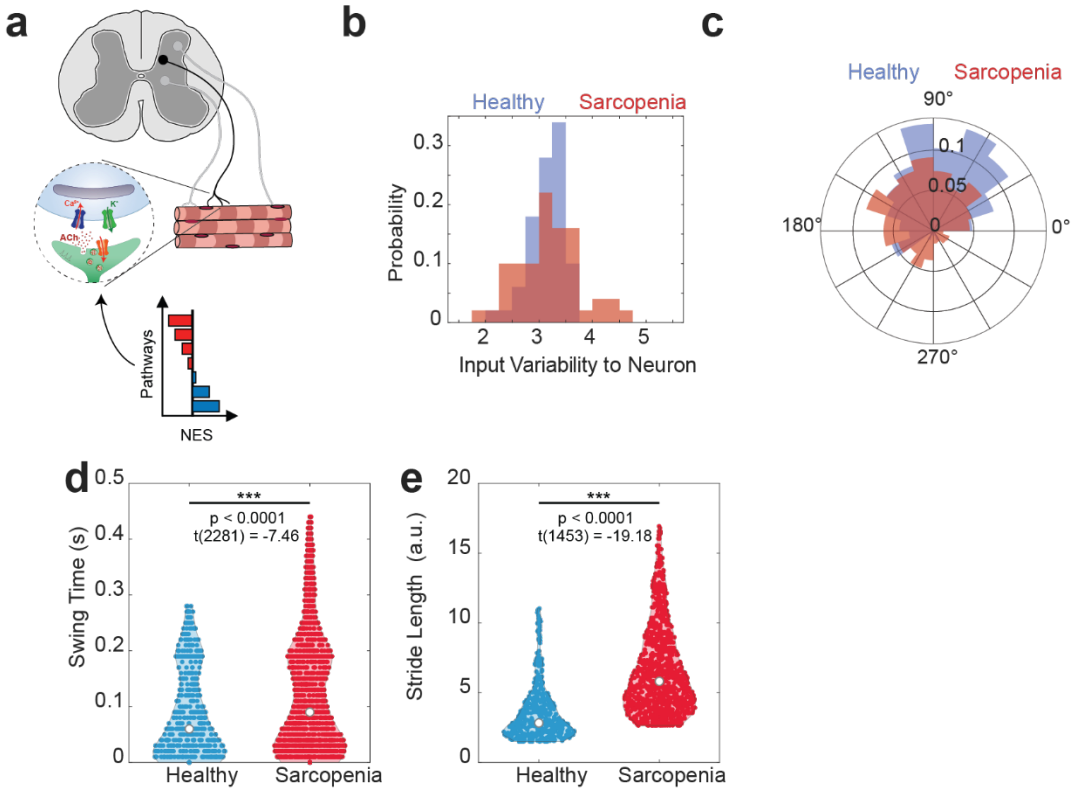

Figure 8. The physiological model illustrates a link between biomolecular determinants and excitation-inhibition balance during space-related sarcopenia. (a) Schematic showing a physiological model of the motor neuron to muscle activation alongside sarcopenia-related gene regulation from normalized enrichment score (NES). **(b)** Probability distribution of modeled input variability to neurons. **(c)** Healthy and sarcopenia population-related phase activity across neurons during inferred muscle activity. Note reduced phase strength during movement. Reported phase coherence for healthy and sarcopenia activity is $R_{healthy}$ = 0.55 and $R_{sarcopenia}$ = 0.33, respectively. **(d)** Modeled swing times of population response under healthy and sarcopenia ($p = 0.00$, $t(1423) = -19.13$, Student's t-test). **(e)** Modeled swing times of population response under healthy and sarcopenia for calculated stride length ($p = 0.00$, $t(2281) = -7.16$, Student's t-test).

This computational framework provided mechanistic insights connecting space-induced alterations in neural excitation/inhibition balance to the observed locomotor deficits. Our findings suggest that space-induced sarcopenia involves not only peripheral muscle atrophy but also fundamental adaptations in neural control systems, including altered central pattern generator function and disrupted coordination between antagonistic

462 muscle groups. These neural adaptations likely contribute significantly to the gait
463 abnormalities documented in our behavioral analysis and highlight potential targets for
464 countermeasure development.
465
466 **DISCUSSION**
467 Space-induced sarcopenia is a major physiological change that affects astronauts. We
468 used transcriptomics muscle biopsies of mice exposed to microgravity and human
469 sarcopenia data to understand the effects of space travel on humans. In this work, we
470 presented a comprehensive framework to understand the biological pathway and its effect
471 on locomotion phenotypes in space-induced sarcopenia. By leveraging TransComp-R,
472 we used a mouse-to-human modeling approach to identify key biological pathways
473 related to neurotransmitter release and regulation, synaptic integration, and mitochondrial
474 dynamics associated with sarcopenia conditions. Likewise, a comprehensive analysis of
475 locomotion behavior in mice exposed to spaceflight showed strong alteration in gait
476 parameters which we mechanistically linked to a CPG network model, incorporating
477 altered identified molecular pathways associated with sarcopenia conditions. Our results
478 established cross-species predictive relationships for studying spaceflight-induced
479 sarcopenia in a framework that links biomolecular determinants of sarcopenia to
480 phenotypically resulting locomotion behavior.
481
482 We identified several immune system pathways altered under conditions of sarcopenia,
483 which has also been observed under spaceflight conditions.[40–42] A study reported immune
484 dysregulation and the redevelopment of herpes virus among astronauts on a 6-month

485 orbital space mission.[43] A separate 6-month spaceflight that studied two crew members
486 identified elevated proinflammatory biomarkers in muscle biopsy post-landing.[44] During
487 spaceflight, blood-derived cytokines including interleukins and tumor necrosis factor-
488 alpha were also significantly elevated during flight.[45] Further investigation of such immune
489 pathways may improve our understanding of spaceflight-induced sarcopenia.
490
491 Metabolic pathways are also actively involved in muscle health as demonstrated by
492 protein alterations during spaceflight.[46] Stein and colleagues reported that whole-body
493 protein synthesis was reduced by 45% about preflight measurements.[47] In the same
494 study, post-flight measurements returned to 91% of the pre-flight levels, indicating a lack
495 of complete recovery from space travel.[47] Additionally, we identified genes that were
496 strongly associated with sarcopenia through neuromuscular signaling. Neuromuscular
497 junction aging has been proposed to be involved in sarcopenia pathogenesis.[48] The age-
498 related denervation at the neuromuscular junction occurs before muscle atrophy[49] and
499 may be involved in sarcopenia pathogenesis.[50]
500
501 We applied a high-throughput drug screening analysis and identified FDA-approved
502 medications that induced gene expression changes potentially linked to protection against
503 or reversing spaceflight-induced sarcopenia. Of the three mouse PCs, we found particular
504 interest in the findings presented on the mouse PC3 due to its ability to explain more
505 variance in human data, indicating the highest potential for mouse-to-human translation.
506 We found a calcium channel blocker (isradipine) and a medication primarily used for
507 myasthenia gravis (mestinon) among the FDA-approved drugs that associated with gene

508 expression changes of a healthy condition. Others have reported that calcium channel
509 blockers like amlodipine[51] and nifedipine[52] are able to attenuate contraction-induced
510 muscle damage muscular atrophy, respectively. A separate study that studied the
511 continuous infusion of mestinon in rats showed improvements to muscle force with
512 treatment post-immobilization-induced muscle weakness.[53] Identifying potential
513 therapeutics may provide insight for future follow-up studies surrounding calcium channel
514 blockers and muscle-strengthening medications.
515
516 The biomechanical alterations we noted in our study from the behavioral assay align with
517 previously documented changes in movement atrophy.[54,55] The propulsion and stride
518 deficits likely reflect preferential atrophy of fast-twitch extensor muscles that generate
519 locomotive force, mirroring the fiber-type selectivity observed in terrestrial sarcopenia but
520 compressed into a remarkably accelerated timeframe (~35 days).[36,56] The concurrent
521 changes in stride parameters suggest simultaneous adaptation of central pattern
522 generators and sensorimotor integration circuits. It is of interest that several key protein
523 pathways were also affected in both humans and mice which could explain some of the
524 downstream locomotion phenotypes. For example, the presence of *DLG3* and *GRIN2B*
525 suggests alterations of synaptic integration across neurons within a CPG network.
526 Interestingly, *GRIN2B* was upregulated in the skeletal muscle of aging mice.[57] Such
527 consequences would be reflected in how neural populations rhythmically generated
528 activity between flexor and extensor periods. Indeed, when altering synaptic integration
529 properties along the network in our CPG model, primarily synaptic release probability and

input gain, we noted a clear reduction in firing coherence between flexor and extensor population, which recapitulates the behavior changes we observed in the gait dynamics.

Although our study identified several pathways to improve our understanding of space-induced sarcopenia, there are limitations to this work. First, due to limited publicly available data on mice that have been exposed to spaceflight, the sample sizes are smaller. Additionally, our mouse and human datasets only contained information from males, which neglects potential biological outcomes in females. Additionally, we only analyzed physiological changes in the quadricep muscle and did not investigate the contribution of other limb muscles. Future studies that incorporate additional demographic and sex-based information of both males and females, with the inclusion of other muscle biopsies and relevant tissue will largely build upon the findings we reported.

Likewise, there are limitations to our computational models. TransComp-R selects homologous gene pairs across mouse and human datasets; thus, genes that do not fit this criterion are omitted. As a result, there is a possibility that these omitted genes may have also served an active role in the physiological changes to spaceflight-induced sarcopenia. Our CPG network model incorporated leaky integrate-and-fire neurons with reciprocal connections, synaptic probabilities, and membrane dynamics. However, additional models can be incorporated to further explore the mechanistic contribution of protein altered during sarcopenia. For example, modeling a biophysically realistic model of neurons with full ion channel distributions and gating dynamics could be more informative on how changes at the protein level affect neural dynamics and CPG activity.

553 For example, one can investigate how excessive synaptic release alters integration
554 properties of neurons and their firing rate. Further experiments are needed to causally
555 link the synaptic and protein interactions to behavioral deficits observed during spaceflight
556 or using alternative models of age-related sarcopenia.
557
558 Our study investigated the effects of sarcopenia resulting from spaceflight travel. We used
559 TransComp-R and identified spaceflight mouse PCs that could predict changes in human
560 age-associated sarcopenia in muscle biopsies. Our findings were then validated by
561 matching a panel of genetic markers from these PCs in other human cohorts across
562 different populations. Lastly, our CPG neuron model, incorporated with changes in cross-
563 species predictive biomarkers of sarcopenia, was able to recapitulate healthy and space-
564 induced sarcopenia phenotypes in locomotion. Thus, our findings in this work pave a path
565 to link molecular pathways to behavioral phenotypes of spaced-induced sarcopenia.
566
567 **MATERIALS AND METHODS**
568 **Data selection**
569 We selected publicly available transcriptomics data from the NASA OSDR and GEO
570 database with the prerequisite that the data contained a balanced number of samples
571 with controls and processed tissue samples from similar quadriceps muscle regions in
572 both mouse and human.
573
574 The mouse dataset was selected from the NASA OSDR. We focused our selection criteria
575 on transcriptomics data that contained muscle samples near the quadriceps. We

576 identified a mouse study (OSD-103) that contained a spaceflight and ground control
577 group. We next searched the GEO database and identified three human sarcopenia
578 datasets with controls and biopsy samples, each containing transcriptomics data of
579 biopsy samples from the vastus lateralis muscle. The datasets represent a demographic
580 population around the world, including Caucasian (GSE111006), Chinese (GSE111016),
581 and Afro-Caribbean (GSE111010).
582
583 **Pre-processing and data normalization**
584 We downloaded human transcriptomics sarcopenia data from the GEO database using
585 the GEO2R platform with Bioconductor tools in R (*GEOquery* ver. 2.70.0, *Biobase* ver.
586 2.62.0, and *limma* ver. 3.58.1). We $\log_2$ transformed the data and z-score normalized the
587 data per gene. We matched the human and mouse datasets for homologous one-to-one
588 gene pairing using the *orthogene* package (ver. 1.8.0). Genes that did not contain
589 homologous pairing were excluded from the model and further downstream analysis.
590
591 **Mouse to human computational modeling**
592 We performed TransComp-R by performing PCA on the mouse space flight with both
593 flight and ground control groups. We selected mouse PCs that explained up to a total of
594 80% cumulative variance to prevent overfitting of the data and inclusion of noise. We
595 projected the human dataset (Chinese cohort GSE111016) into the mouse PC space.
596 The projection of the human data into the mouse PCA space is a matrix multiplication of
597 $X^{s \times n}$ and $Q^{n \times p}$ such that *s* is the row of human patients, *n* is the homologous gene pairs

shared across both mouse and human, and *p* is the number of PCs that explain 80% cumulative variance. The equation is also shown:

$$P^{s\,x\,p} = X^{s\,x\,n} Q^{n\,x\,p} \quad (1)$$

Feature selection of mouse principal components

To select important features and regularize the mouse PCs that best predicted human sarcopenia condition, we performed LASSO across 20 rounds of 5-fold cross-validations by regressing the human sarcopenia and control group positions along the mouse PCA space against the human disease condition. Mouse PCs with a non-zero coefficient frequency greater than 10 of 20 rounds were selected for the generalized linear model. We performed the generalized linear regression using the equation:

$$Y \sim \beta_0 + \sum_{i=1}^{k} \beta_i (X q_i) \quad (2)$$

In the generalized linear model, the Xq_i represents the projected human samples into mouse PCs that were selected by LASSO and *Y* is the human sarcopenia and control status. We selected mouse PCs with a p value less than 0.05 for downstream biological interpretation.

Variance explained in human by mouse principal components

Using principal components encoding mouse variation and human data, we can calculate how much variation the mouse PCs explain the variation in humans. We calculated the variance explained by mouse PCs in human data with the equation:

$$VarExpHuman(q_i) = \frac{q_i^T [X^T X] q_i}{sum(diag[Q^T X^T X Q])} \quad (3)$$

620 Where $X^{s \times n}$ is a human data matrix represented by *s* number of subjects and *n* number
621 of genes, and $Q^{n \times p}$ is the mouse data represented by the loading coefficients of *n* number
622 genes and *p* columns of principal components q_i. The *T* represents the transpose of the
623 data matrix.
624

625 **Gene set enrichment analysis**

626 We selected PCs that significantly distinguished between human sarcopenia and control
627 groups for downstream pathway analysis. To identify enriched pathways, we pre-ranked
628 each significant PC by their respective loadings score and performed GSEA in R (*msigdbr*
629 ver. 7.5.1, *fgsea* ver. 1.28.0, *clusterProfiler* ver. 4.10.1).[58–60] We generated a holistic
630 understanding of the enriched pathways by using the hallmark and KEGG curations from
631 the Molecular Signatures Database. The parameters we used to identify enriched
632 biological pathways included a minimum gene size of 5, a maximum gene size of 500,
633 and an epsilon value of 0. We used the default parameter of 1000 permutations to
634 determine the statistical significance. We defined biological pathways in both KEGG and
635 hallmark to be significant if the Benjamini-Hochberg adjusted p value was less than 0.01.
636

637 **Gene selection for cross-population validation**

638 To ensure our findings are reproducible in other datasets, we used the Caucasian and
639 Afro-Caribbean datasets (GSE111006 and GSE111010) to determine if the findings in
640 the Chinese cohort are reflective in other demographics. In both the Caucasian and Afro-
641 Caribbean datasets, we first excluded control patients with a reported history of low
642 muscle mass or low muscle strength and/or performance to ensure the control groups

643 had no potential complications. We then concomitantly merged the two cohorts into a
644 singular dataset and verified for batch effects visualized by PCA.
645
646 Using the Chinese cohort, we filtered for the top 10 and bottom 10 gene loadings from
647 significant mouse PCs identified in our TransComp-R model to determine if transcriptomic
648 variation encoded on these PCs could stratify sarcopenia and healthy groups in the
649 Caucasian and Afro-Caribbean populations.
650
651 **Partial least squares discriminant analysis**
652 We used the *mixOmics* package (ver. 6.26.0) to construct the PLS-DA models for each
653 significant mouse PC that could significantly stratify human sarcopenia and control groups
654 in the Chinese sarcopenia cohort.[61]
655
656 We identified the most important genes contributing to the model's predictive ability by
657 calculating the VIP scores. We used the *mixOmics* package to calculate the VIP scores
658 for each given LV. The following equation:

659 $$VIP_k = \sqrt{\frac{K \sum_{a=1}^{A} w_{ak}^2 SSA_a}{A \cdot SSA_{total}}} \quad (\mathbf{4})$$

660 A given VIP score for a specific gene is calculated by *K* number of genes, *A* number of
661 PLS-DA components, and w_{ak} weight of the gene *k* in a^{th} LV. SSA_a and SSA_{total} are the
662 sum of squares in the ath LV and the total sum of squares in all LV components,
663 respectively. We defined a VIP score greater than 1 to represent genes contributing
664 above average to the model's performance.
665

666 **In silico cross-species drug screening analysis**

667 We computationally screened for drugs correlated with the mouse PCs predictive of
668 sarcopenia for therapeutic potential. We used the L1000 Consensus Signatures
669 Coefficient Tables (Level 5) from the LINCS database. Prior to data use, we referred to
670 the LINCS small molecules metadata and removed all the drugs that did not report any
671 known targets. To identify candidate drugs with potential therapeutic connections to
672 sarcopenia, we integrated the differentially expressed genes (DEGs) from each drug in
673 the LINCS database and the gene loadings from the mouse PCs predictive of human
674 sarcopenia. The DEGs for each drug were selected by scaling the characteristic direction
675 coefficients, the up- or down-regulation of a gene by the drug, to z-scores and obtaining
676 genes, and their characteristic direction values, with p-value < 0.05.[31]

677

678 We paired the genes of the mouse PC loadings with the differentially expressed drug
679 genes and performed Spearman's correlation. We selected correlations that had a
680 Benjamini-Hochberg adjusted *p* value less than 0.05. Based on the Spearman's rho
681 value, we ranked the drugs for each mouse PC that was processed.

682

683 **Multivariate analysis of locomotor behavior**

684 We used the OSD-478 from the NASA OSDR for locomotor behavior analysis. Principal
685 component analysis was applied to 47 locomotor behavioral parameters measured in
686 n=35 C57BL/6J mice across four experimental groups: pre-flight spaceflight (pre-flight),
687 post-flight spaceflight (post-flight), pre-flight ground control (GC pre), and post-flight
688 ground control (GC post). Parameters included stride kinematics (length, duration,

variability), limb coordination metrics, and ground reaction forces collected during treadmill locomotion.

Behavior and spaceflight cluster validation

All behavioral and locomotion analysis was performed using MATLAB. Group separation was visualized in reduced-dimensional space by projecting z-scored data onto the first three PCs. We calculated 95% confidence ellipses for each experimental group using:

$$Cluster\ radius = \chi 2_{(0.95,22)} \cdot \lambda_i \quad (\mathbf{5})$$

where χ=5.991 and λ_i represents the eigenvalue of the ith PC. Multivariate analysis of variance (ANOVA) with Hotelling's T^2 post-hoc tests assessed group differences in PC space (α=0.05, Bonferroni-corrected).

Feature selection and hypothesis testing

Behavioral variables most associated with spaceflight effects were identified by examining PC loadings. For each of the first three PCs, we selected variables with absolute loadings exceeding the 95th percentile of loading magnitudes (equivalent to the top 5 variables per PC).

Motor neuron population model for movement

To model motor neuron population for biophysical extraction of movement, we simulated a population of 50 leaky integrate-and-fire neurons with equal proportions of flexor and extensor connectivity to muscle output. Membrane potential dynamics followed biophysically realistic neurons (**Table 1**). Neuronal populations between extensor and

flexors were reciprocally connected with inhibitory conductance, generating coupled generation of spiking activity resembling pattern generation circuits (CPG) for locomotion.

Table 1. Parameters for the CPG model

Variable	Value
Resting potential (mV)	-65
Reset potential (mV)	-70
Membrane resistance (MΩ)	10
Synaptic conductance (nS)	0.4
Inhibitory reversal potential (mV)	-80
Synaptic decay (ms)	5
Mean membrane time constant (ms)	10
Refractory period (ms)	3

We also incorporated "kick and decay" kinetics during reciprocal inputs of neuronal populations. Together the change in voltage for each neuron was characterized as:

$$\tau m\, dV/dt = -(V - E_L) + R_m I(t) \quad (\mathbf{6})$$

where τm is the membrane time constant, V is the membrane potential, E_L is the leak reversal potential, $R_m$is the membrane resistance and $I(t)$ is the input current as a function of time.

Inference of locomotory activity

Population firing rate activity was temporally smoothed with a 5 ms Gaussian kernel. Peak population activity bursts between flexor and extensor neurons were used to calculate the phase difference and cycle lengths which were used to infer stride length and variability, respectively. The correlation of variation was calculated by taking the mean and standard deviation of cycle lengths between population bursts. To infer swing times, the duration of peak responses in the flexor population was calculated and the differences were taken for each cycle. Similarly, the stance time was taken as the time from the end of the

731 previous swing cycle and the next swing cycle. The ratio of both swing and stance times
732 yielded the swing stance ratio.
733
734 **REFERENCES**

735 1. Yatagai, F., Honma, M., Dohmae, N. & Ishioka, N. Biological effects of space
736 environmental factors: A possible interaction between space radiation and
737 microgravity. *Life Sciences in Space Research* **20**, 113–123 (2019).
738 2. Chancellor, J. C., Scott, G. B. I. & Sutton, J. P. Space Radiation: The Number One
739 Risk to Astronaut Health beyond Low Earth Orbit. *Life (Basel)* **4**, 491–510 (2014).
740 3. Cucinotta, F. A. Space Radiation Risks for Astronauts on Multiple International Space
741 Station Missions. *PLOS ONE* **9**, e96099 (2014).
742 4. Willey, J. S. *et al.* The individual and combined effects of spaceflight radiation and
743 microgravity on biologic systems and functional outcomes. *Journal of Environmental*
744 *Science and Health, Part C* **39**, 129–179 (2021).
745 5. Le, H., Rai, V. & Agrawal, D. K. Cholesterol: An Important Determinant of Muscle
746 Atrophy in Astronauts. *Journal of Biotechnology and Biomedicine* **6**, 67–79 (2023).
747 6. Trappe, T. A., Tesch, P., Alkner, B. & Trappe, S. Microgravity-induced skeletal muscle
748 atrophy in women and men: implications for long-duration spaceflights to the Moon
749 and Mars. *Journal of Applied Physiology* **135**, 1115–1119 (2023).
750 7. Dhillon, R. J. & Hasni, S. Pathogenesis and Management of Sarcopenia. *Clin Geriatr*
751 *Med* **33**, 17–26 (2017).

752 8. Takahashi, H., Nakamura, A. & Shimizu, T. Simulated microgravity accelerates aging
753 of human skeletal muscle myoblasts at the single cell level. *Biochemical and*
754 *Biophysical Research Communications* **578**, 115–121 (2021).
755 9. Larsson, L. *et al.* Sarcopenia: Aging-Related Loss of Muscle Mass and Function.
756 *Physiological Reviews* **99**, 427–511 (2019).
757 10. Corlett, T., Stavnichuk, M. & Komarova, S. V. Population analysis of space travelers.
758 *Life Sciences in Space Research* **27**, 1–5 (2020).
759 11. Kunitskaya, A., Piret, J. M., Buckley, N. & Low-Décarie, E. Meta-analysis of health
760 research data from greater than three months International Space Station missions.
761 *Acta Astronautica* **201**, 420–430 (2022).
762 12. Kim, S., Ayan, B., Shayan, M., Rando, T. A. & Huang, N. F. Skeletal muscle-on-a-chip
763 in microgravity as a platform for regeneration modeling and drug screening. *Stem Cell*
764 *Reports* **19**, 1061–1073 (2024).
765 13. Baek, K.-W. *et al.* Rodent Model of Muscular Atrophy for Sarcopenia Study. *J Bone*
766 *Metab* **27**, 97–110 (2020).
767 14. Brubaker, Douglas. K. *et al.* An interspecies translation model implicates integrin
768 signaling in infliximab-resistant inflammatory bowel disease. *Sci Signal* **13**, eaay3258
769 (2020).
770 15. Brubaker, D. K. & Lauffenburger, D. A. Translating preclinical models to humans.
771 *Science* **367**, 742–743 (2020).
772 16. Bergendorf, A., Park, J. H., Ball, B. K. & Brubaker, D. K. Mouse-to-human modeling
773 of microglia single-nuclei transcriptomics identifies immune signaling pathways and

774 potential therapeutic candidates associated with Alzheimer's disease.
775 2025.02.07.637100 Preprint at https://doi.org/10.1101/2025.02.07.637100 (2025).
776 17. Ball, B. K., Kuhn, M. K., Fleeman Bechtel, R. M., Proctor, E. A. & Brubaker, D. K.
777 Differential responses of primary neuron-secreted MCP-1 and IL-9 to type 2 diabetes
778 and Alzheimer's disease-associated metabolites. *Sci Rep* **14**, 12743 (2024).
779 18. Ball, B. K., Proctor, E. A. & Brubaker, D. K. Cross-Species Modeling Identifies Gene
780 Signatures in Type 2 Diabetes Mouse Models Predictive of Inflammatory and
781 Estrogen Signaling Pathways Associated with Alzheimer's Disease Outcomes in
782 Humans. in *Biocomputing 2025* 426–440 (WORLD SCIENTIFIC, 2024).
783 doi:10.1142/9789819807024_0031.
784 19. Lee, M. J. *et al.* Computational Interspecies Translation Between Alzheimer's Disease
785 Mouse Models and Human Subjects Identifies Innate Immune Complement,
786 TYROBP, and TAM Receptor Agonist Signatures, Distinct From Influences of Aging.
787 *Frontiers in Neuroscience* **15**, (2021).
788 20. Ball, B. K., Park, J. H., Bergendorf, A. M., Proctor, E. A. & Brubaker, D. K. Translational
789 disease modeling of peripheral blood identifies type 2 diabetes biomarkers predictive
790 of Alzheimer's disease. *npj Syst Biol Appl* **11**, 1–16 (2025).
791 21. Suarez-Lopez, L. *et al.* Cross-species transcriptomic signatures predict response to
792 MK2 inhibition in mouse models of chronic inflammation. *iScience* **24**, 103406 (2021).
793 22. Harris-Warrick, R. M. Neuromodulation and flexibility in Central Pattern Generator
794 networks. *Curr Opin Neurobiol* **21**, 685–692 (2011).
795 23. Grillner, S. & El Manira, A. Current Principles of Motor Control, with Special Reference
796 to Vertebrate Locomotion. *Physiol Rev* **100**, 271–320 (2020).

797 24. Beheshti, A., Ray, S., Fogle, H., Berrios, D. & Costes, S. V. A microRNA signature and
798 TGF-β1 response were identified as the key master regulators for spaceflight
799 response. *PLoS One* **13**, e0199621 (2018).
800 25. McDonald, J. T. *et al.* NASA GeneLab Platform Utilized for Biological Response to
801 Space Radiation in Animal Models. *Cancers (Basel)* **12**, 381 (2020).
802 26. Migliavacca, E. *et al.* Mitochondrial oxidative capacity and NAD+ biosynthesis are
803 reduced in human sarcopenia across ethnicities. *Nat Commun* **10**, 5808 (2019).
804 27. Membrez, M. *et al.* Trigonelline is an NAD+ precursor that improves muscle function
805 during ageing and is reduced in human sarcopenia. *Nat Metab* **6**, 433–447 (2024).
806 28. Lim, S. C. *et al.* Mutations in LYRM4, encoding iron–sulfur cluster biogenesis factor
807 ISD11, cause deficiency of multiple respiratory chain complexes. *Hum Mol Genet* **22**,
808 4460–4473 (2013).
809 29. Mori, F. *et al.* Genetic variants of the NMDA receptor influence cortical excitability and
810 plasticity in humans. *Journal of Neurophysiology* **106**, 1637–1643 (2011).
811 30. Akashi, K. *et al.* NMDA Receptor GluN2B (GluRε2/NR2B) Subunit Is Crucial for
812 Channel Function, Postsynaptic Macromolecular Organization, and Actin
813 Cytoskeleton at Hippocampal CA3 Synapses. *J Neurosci* **29**, 10869–10882 (2009).
814 31. Xie, Z. *et al.* Getting Started with LINCS Datasets and Tools. *Curr Protoc* **2**, e487
815 (2022).
816 32. Ahmadian, M. *et al.* PPARγ signaling and metabolism: the good, the bad and the
817 future. *Nat Med* **19**, 557–566 (2013).
818 33. Kwok, A. *et al.* Altered rodent gait characteristics after ~35 days in orbit aboard the
819 International Space Station. *Life Sciences in Space Research* **24**, 9–17 (2020).

820 34. Sundaramurthy, A. *et al.* Effect of stride length on the running biomechanics of healthy
821 women of different statures. *BMC Musculoskelet Disord* **24**, 604 (2023).
822 35. MULAVARA, A. P. *et al.* Physiological and Functional Alterations after Spaceflight and
823 Bed Rest. *Med Sci Sports Exerc* **50**, 1961–1980 (2018).
824 36. Fitts, R. H., Riley, D. R. & Widrick, J. J. Functional and structural adaptations of
825 skeletal muscle to microgravity. *J Exp Biol* **204**, 3201–3208 (2001).
826 37. Marder, E. & Bucher, D. Central pattern generators and the control of rhythmic
827 movements. *Curr Biol* **11**, R986-996 (2001).
828 38. Dayan, P. & Abbott, L. F. *Theoretical Neuroscience: Computational and Mathematical*
829 *Modeling of Neural Systems*. (MIT Press, Cambridge, Mass., 2001).
830 39. Trappenberg, T. *Fundamentals of Computational Neuroscience*. (OUP Oxford, 2010).
831 40. Smith, J. K. IL-6 and the dysregulation of immune, bone, muscle, and metabolic
832 homeostasis during spaceflight. *npj Microgravity* **4**, 1–8 (2018).
833 41. Okamura, Y. *et al.* Impact of microgravity and lunar gravity on murine skeletal and
834 immune systems during space travel. *Sci Rep* **14**, 28774 (2024).
835 42. An, R. *et al.* Influence of the spaceflight environment on macrophage lineages. *npj*
836 *Microgravity* **10**, 1–8 (2024).
837 43. Rooney, B. V., Crucian, B. E., Pierson, D. L., Laudenslager, M. L. & Mehta, S. K.
838 Herpes Virus Reactivation in Astronauts During Spaceflight and Its Application on
839 Earth. *Front Microbiol* **10**, 16 (2019).
840 44. Capri, M. *et al.* Recovery from 6-month spaceflight at the International Space Station:
841 muscle-related stress into a proinflammatory setting. *FASEB J* **33**, 5168–5180 (2019).

842 45. Crucian, B. *et al.* Immune System Dysregulation Occurs During Short Duration
843 Spaceflight On Board the Space Shuttle. *J Clin Immunol* **33**, 456–465 (2013).
844 46. Ferrando, A. A., Paddon-Jones, D. & Wolfe, R. R. Alterations in protein metabolism
845 during space flight and inactivity. *Nutrition* **18**, 837–841 (2002).
846 47. Stein, T. P., Leskiw, M. J., Schluter, M. D., Donaldson, M. R. & Larina, I. Protein
847 kinetics during and after long-duration spaceflight on MIR. *American Journal of*
848 *Physiology-Endocrinology and Metabolism* **276**, E1014–E1021 (1999).
849 48. Moreira-Pais, A., Ferreira, R., Oliveira, P. A. & Duarte, J. A. A neuromuscular
850 perspective of sarcopenia pathogenesis: deciphering the signaling pathways
851 involved. *GeroScience* **44**, 1199–1213 (2022).
852 49. Deschenes, M. R., Roby, M. A., Eason, M. K. & Harris, M. B. Remodeling of the
853 neuromuscular junction precedes sarcopenia related alterations in myofibers.
854 *Experimental Gerontology* **45**, 389–393 (2010).
855 50. Arnold, W. D. & Clark, B. C. Neuromuscular junction transmission failure in aging and
856 sarcopenia: The nexus of the neurological and muscular systems. *Ageing Research*
857 *Reviews* **89**, 101966 (2023).
858 51. Beaton, L. J., Tarnopolsky, M. A. & Phillips, S. M. Contraction-induced muscle damage
859 in humans following calcium channel blocker administration. *J Physiol* **544**, 849–859
860 (2002).
861 52. Wagatsuma, A., Fujimoto, K. & Yamada, S. Effect of treatment with nifedipine, an L-
862 type calcium channel blocker, on muscular atrophy induced by hindlimb
863 immobilization. *Scandinavian Journal of Medicine & Science in Sports* **12**, 26–30
864 (2002).

865 53. Frick, C. G., Helming, M., Martyn, J. A. J., Blobner, M. & Fink, H. Continuous
866 administration of pyridostigmine improves immobilization-induced neuromuscular
867 weakness. *Critical Care Medicine* **38**, 922 (2010).
868 54. Furukawa, S. *et al.* Findings from recent studies by the Japan Aerospace Exploration
869 Agency examining musculoskeletal atrophy in space and on Earth. *npj Microgravity*
870 **7**, 1–10 (2021).
871 55. Lee, P. H. U., Chung, M., Ren, Z., Mair, D. B. & Kim, D.-H. Factors mediating
872 spaceflight-induced skeletal muscle atrophy. *American Journal of Physiology-Cell*
873 *Physiology* **322**, C567–C580 (2022).
874 56. Rowan, S. L., Purves-Smith, F. M., Solbak, N. M. & Hepple, R. T. Accumulation of
875 severely atrophic myofibers marks the acceleration of sarcopenia in slow and fast
876 twitch muscles. *Experimental Gerontology* **46**, 660–669 (2011).
877 57. Endo, Y. *et al.* Exercise-induced gene expression changes in skeletal muscle of old
878 mice. *Genomics* **113**, 2965–2976 (2021).
879 58. Dolgalev, I. msigdbr: MSigDB Gene Sets for Multiple Organisms in a Tidy Data
880 Format. (2022).
881 59. Korotkevich, G. *et al.* Fast gene set enrichment analysis. 060012 Preprint at
882 https://doi.org/10.1101/060012 (2021).
883 60. Yu, G., Wang, L.-G., Han, Y. & He, Q.-Y. clusterProfiler: an R Package for Comparing
884 Biological Themes Among Gene Clusters. *OMICS: A Journal of Integrative Biology*
885 **16**, 284–287 (2012).

61. Rohart, F., Gautier, B., Singh, A. & Cao, K.-A. L. mixOmics: An R package for 'omics feature selection and multiple data integration. *PLOS Computational Biology* **13**, e1005752 (2017).

ACKNOWLEDGEMENTS

BKB and HFK is supported by the NSF GRFP (DGE-1842166). DDC is supported in part by the DARPA Young Faculty Award (Army Research Office Contract W911NF21103272) and National Science Foundation (Awards 1944394 and 2149946). DKB is supported by an award from the Good Ventures Foundation, Open Philanthropy, and start-up funds from Case Western Reserve University.

AUTHOR CONTRIBUTIONS

BKB: Conceptualization, data curation, formal analysis, investigation, methodology, visualization, writing-original draft, writing-review & editing. HFK: Conceptualization, data curation, formal analysis, investigation, methodology, visualization, writing-original draft, writing-review & editing. JHP: Data curation, methodology, writing-review & editing. KJ: Project administration, resources, writing-review & editing. DDC: Conceptualization, methodology, project administration, resources, funding acquisition, writing-review & editing. DKB: Conceptualization, funding acquisition, methodology, project administration, resources, writing-review & editing.

DATA AVAILABILITY

All human transcriptomics data used from the study is available through Gene Expression Omnibus with accession numbers GSE111006, GSE111010, and GSE111016. Mouse transcriptomics data is available through the NASA Open Science Data Repository with accession OSD-103. Mouse behavioral data is available with accession OSD-478 on the NASA OSDR.

SUPPLEMENTARY INFORMATION AND CODE AVAILABILITY

All code used for the analysis is available at https://github.com/Brubaker-Lab/MouseFLTandHumanSA. All supplementary information including figures and data is also made available on the GitHub repository.

COMPETING INTERESTS

The authors declare no competing interests.

932 **SUPPLEMENTARY INFORMATION**

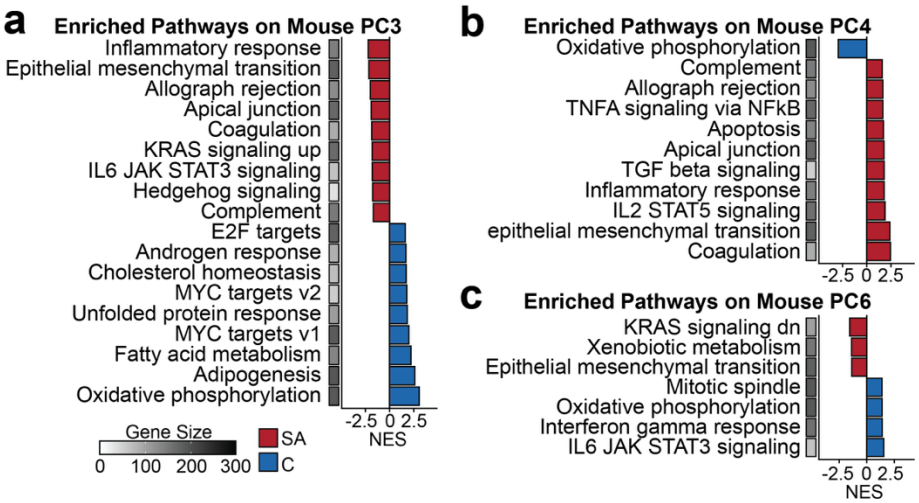

933

934 **Supplementary Figure 1. Hallmark pathway enrichment analysis. (a)** Significantly
935 enriched pathways on mouse PC3, **(b)** PC4, and **(c)** PC6. (SA=sarcopenia, C=control).
936

937

938

939

940

941

942

943

944

945

946

947

948

949

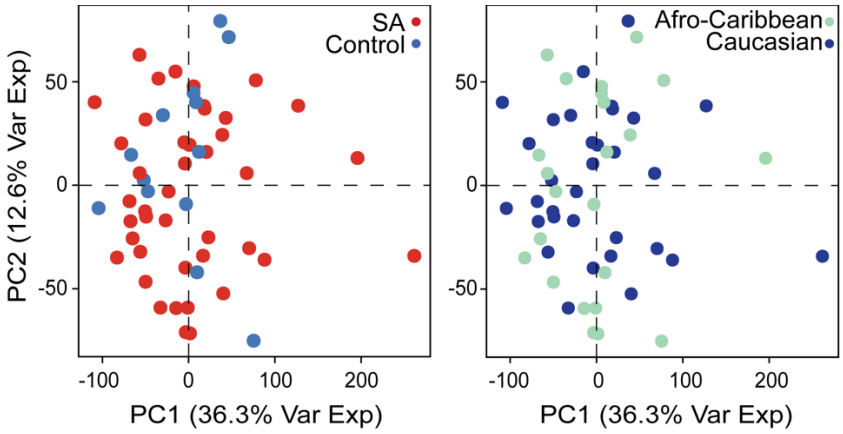

Supplementary Figure 2. Principal component analysis of the merged Afro-Caribbean and Caucasian dataset. Human patients are labeled by their disease condition and their association with a demographic cohort (SA=sarcopenia).

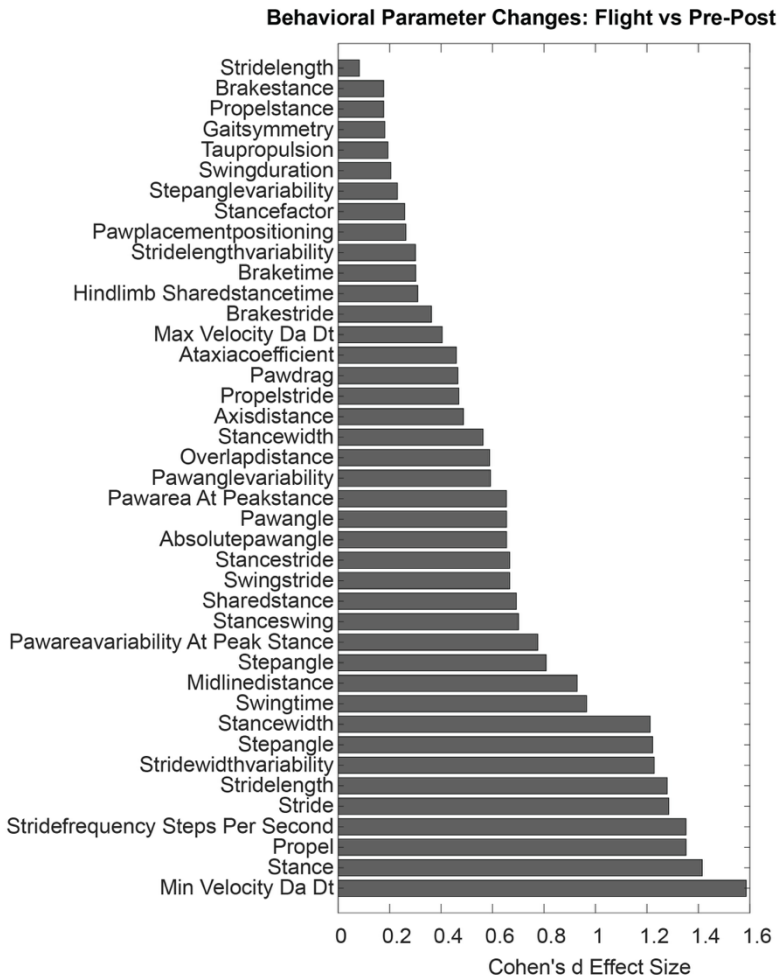

Supplementary Figure 3. Effect size of behaviors pre- and post-flight. All gait parameter effect sizes were calculated between pre- and post-flight time points.